Bull. Mater. Sci., Vol. 39, No. 5, September 2016, pp. 1303–1309. © Indian Academy of Sciences.
DOI 10.1007/s12034-016-1277-9

Understanding the effect of *n*-type and *p*-type doping in the channel of graphene nanoribbon transistor

SUDHANSHU CHOUDHARY* and VIKRAM SINGH
School of VLSI Design and Embedded Systems, NIT Kurukshetra, Kurukshetra 136 119, India

MS received 23 July 2015; accepted 19 October 2015

Abstract. **In this paper, device performance of graphene nanoribbon field effect transistor (GNRFET) with different doping concentrations in different parts of the channel is reported. The study is performed by using atomistic simulations based on self-consistent solution of Schrodinger's and Poisson's equation within the non-equilibrium Green's function formalism. The transfer and output characteristics suggest that device performance with *n*-type doping in the channel is better with smaller supply voltage compared to higher supply voltage. On increasing the *n*-type doping concentration, we obtained better on-current and output characteristics in comparison with undoped and *p*-type doped channel GNRFET. Further, we introduced step-doping profile in the graphene nanoribbon (GNR) channel and found that the device gives better on-current and good saturation condition when compared to undoped or uniformly-doped channel.**

Keywords. **Doping; graphene; field-effect transistor; graphene nanoribbon.**

1. Introduction

During the previous few years, various properties of carbon nanostructures have attracted more research because of its variable electrical properties, which can be utilized for various electronic applications. Graphene nanoribbon (GNR) presents a new approach for different devices. In past, huge efforts have been done by the researchers to understand the electrical properties of GNR. In 2-D graphene sheet, electrons behave as massless charge carriers [1] which travel through the lattice with a long relaxation path [2]. Graphene has zero bandgap structure, which makes it unsuitable for switching applications. However, the energy bandgap can be created by lateral confinement of the particle [3].

It has been proved earlier that on varying the width of the GNR sheet, energy gap will vary which has an inverse relation to each other [4,5]. Graphene nanoribbon field effect transistor (GNRFET) can be fabricated by connecting the GNR channel with metal contacts [6,7], therefore, obtaining a well-known Schottky-barrier FET (SBFET). Fabrication techniques are available; however, simulations are equally important before fabrication. Simulations can give a detailed analysis and characteristics of the device being fabricated. Quantum simulations based on tight-binding approach [8,9] are used to assess device potential. This approach is based on the 3-D Poisson's and Schrodinger's equation solver within the non-equilibrium Green's function (NEGF) calculation [10]. In GNR, different types of nonlinearities arise due to a cavity, an ionized impurity in the channel and edge cavities [8,9]. Doped impurity in different parts of channel may give better GNRFET characteristics and hence are interesting to investigate. In this paper, we investigate the effect of doping of the GNRFET channel on the device characteristics.

2. Model and method

Device characteristics of GNRFET are calculated by solving the 3-D Poisson's and Schrodinger's equation using the NEGF formulation-based software called NanoTCAD-Vides [11]. A tight binding Hamiltonian is used to describe the atomistic details of the GNR channel. Figure 1a shows a schematic arrangement of GNRSBFET with contact SB height of $\Phi_{Bn} = \Phi_{Bp} = E_g/2$.

Double gate geometry with SiO_2 thickness of 1.5 nm and dielectric constant 3.9 is used in the simulations. A 9 nm long, $N = 9$ smooth GNR channel that has a width of 2.1 nm is considered at room temperature. Power supply voltage, $V_{DD} = 0.5$ V [12,13].

A 9 nm GNR channel is divided into three regions as shown in figure 1b in which first region is 0–3 nm long, second region is 3–6 nm long and third region is 6–9 nm long, and in these three regions *n*-type and *p*-type dopings are varied. *n*-type and *p*-type dopings act as fixed charge in particular region, which play an important role in the variation of electrostatic potential of the device. A self-consistent, repetitive loop solves the transport equation and 3-D Poisson's equation.

*Author for correspondence (hellosudhanshubit@gmail.com)

3. Results and discussion

The impact of doping on the electronic movement, such as carrier mobility is not yet clear. In this section, we study doping performance of the device and its limitations. The quantum transport equation is solved using NEGF for narrow GNR (0–9 nm). The doping limited mobility is inversely proportional to the doping in different regions [6]. We first obtain results for a GNR-SBFET without doping, which is shown in figure 2a and b.

We observed low values of I_{on} and I_{off} currents from figure 2a and b, and are provided in table 1, which is due to limited free π electron. To improve the performance of the device, n-type and p-type dopings have been introduced in different parts of the channel, n-type and p-type doping profiles increase free charge career in the channel due to which we can see large variations in on- and off-currents. Considering the fact that electrons are lighter and faster than holes, n-type doping of the channel is expected to enhance on-current for any type of metal-semiconductor contact. The effect of

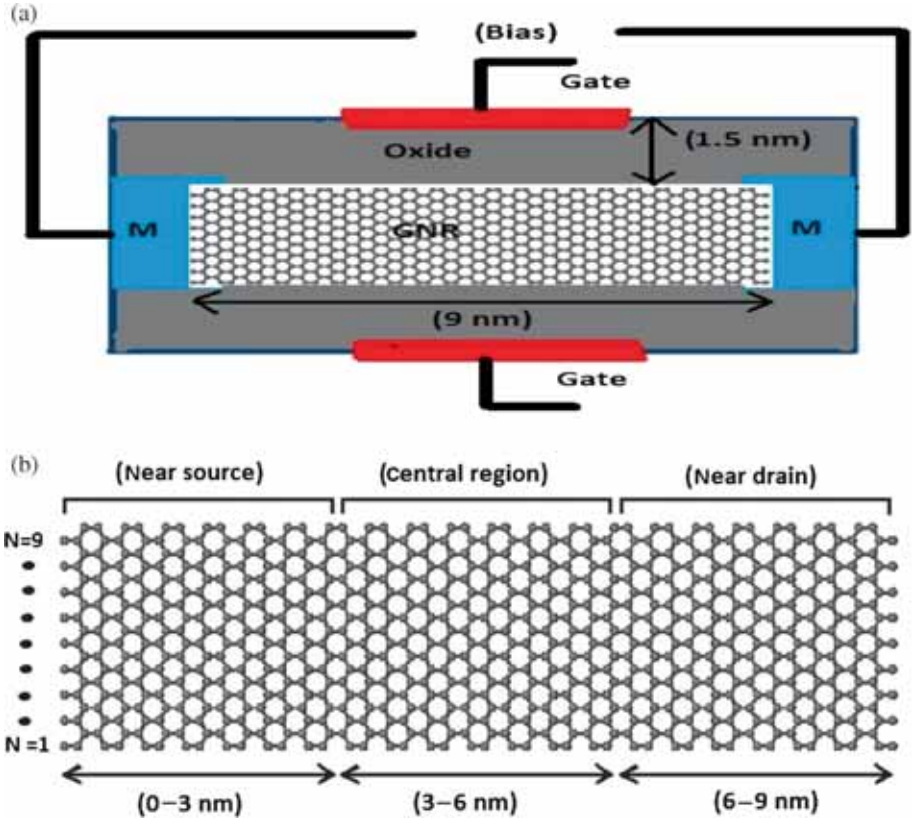

Figure 1. (**a**) GNR-SBFET with metal contact and (**b**) GNR channel with different three divided regions.

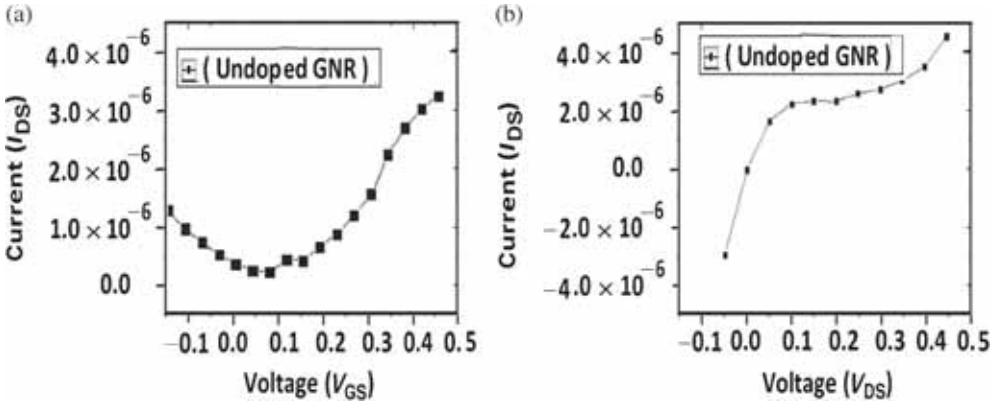

Figure 2. Current I_{DS} in amperes and voltages V_{GS} and V_{DS} in volts. (**a**) Transfer and (**b**) output characteristics of GNR-SBFET without doping.

variable n-type and p-type doping concentrations in 0–3 nm region of a 9 nm channel length device is evaluated and its transfer and output characteristics are shown in figures 3 and 4.

From the transfer and output characteristics of figures 3 and 4 (for 0–3 nm region), we find off-current (I_{off}) at $V_{GS} = -V_{DD}$ and $V_{DS} = V_{DD}$, and on-current (I_{on}) at $V_{GS} = V_{DS} = V_{DD}$, which are shown in table 2. From table 2, we observe that p-type channel gives more off-current in comparison to n-type-doped channel. It is also observed that n-type-doped structure gives larger on-current with respect to undoped channel device. Further, we consider doping in another region (3–6 nm region) and calculated its transfer and output characteristics (see figures 5 and 6) by varying n-type and p-type doping concentrations in this region.

Table 1. I_{on} and I_{off} currents of undoped GNR channel.

Doping concentration	I_{on} (Amp)	I_{off} (Amp)
Ideal GNR (Zero doping con.)	3.01×10^{-6}	2.92×10^{-6}

It was observed that on increasing doping concentration in this region, I_{on} increases marginally and I_{off} decreases marginally, I_{on}/I_{off} ratio remains almost same. Next, we consider 6–9 nm region with variable n-type and p-type dopings and calculate its transfer and output characteristics in figures 7 and 8, which shows that saturation condition takes place in n-type-doped channel, however, p-type-doped channel device remains unsaturated.

On comparing figures 2–8, we observe larger variations in on and off-currents in n-type-doped structure in comparison with p-type-doped and undoped channel structures. It is also possible to obtain the important saturation characteristics on introducing n-type-doping near drain side, which further improves with increase in doping concentration. For a more general analysis, we have calculated I_{on} and I_{off} currents from input and output characteristics for all the structures, which are shown in table 2. Switching is the most important characteristic to achieve graphene-based electronic devices with high performance, finite bandgap (E_g) graphene sheets are usually required for different electronic applications. I_{on}/I_{off} ratio in FETs is dependent on E_g of the

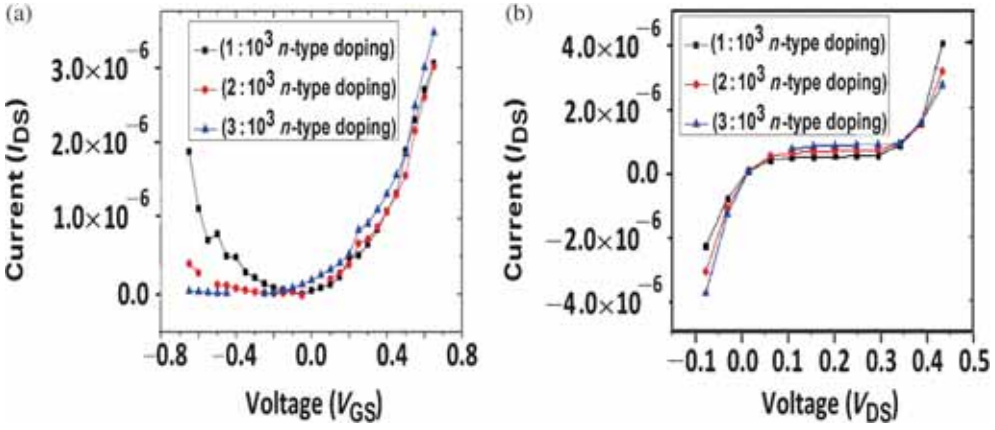

Figure 3. Current I_{DS} in amperes and voltages V_{GS} and V_{DS} in volts. (**a**) Transfer and (**b**) output characteristics of GNR-SBFET with n-type doping in 0–3 nm region of a 9 nm channel.

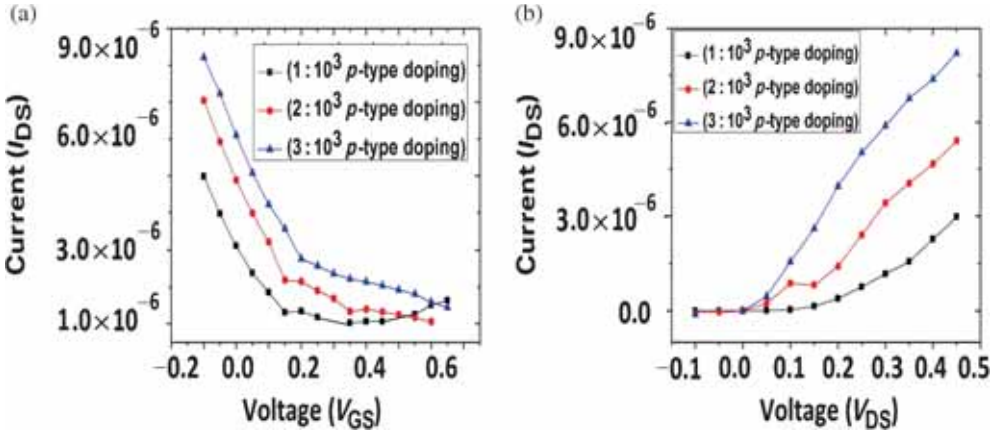

Figure 4. Current I_{DS} in amperes and voltages V_{GS} and V_{DS} in volts. (**a**) Transfer and (**b**) output characteristics of GNR-SBFET with p-type doping in 0–3 nm (near source) region of a 9 nm channel.

channel material on the basis of the following proportional relationship:

$$I_{on}/I_{off} \propto e^{E_g/K_BT}.$$

The variation in I_{on}/I_{off} ratio suggests the variation in bandgap of graphene sheet channel (from the above relation). From tables 1 and 2, we observed that undoped channel gives less on-current compared to doped channel. On introducing low ($1{:}10^3$) n-type doping concentration in 6–9 nm region, I_{on} current reduces when compared to high-doped concentration ($3{:}10^3$) structure. Thus, in undoped SBFET, due to higher barrier at the interface, I_{on} current reduces. On increasing the impurity carrier concentration and when the gate voltage is increased, barrier reduces and

Table 2. I_{on} and I_{off} currents of doped GNR channel.

Doping concentration	I_{on} (Amp) n-type	I_{on} (Amp) p-type	I_{off} (Amp) n-type	I_{off} (Amp) p-type
$1{:}10^3$ (0–3 nm region)	3.7×10^{-6}	2.5×10^{-6}	3.1×10^{-6}	1.2×10^{-6}
$2{:}10^3$ (0–3 nm region)	5.9×10^{-6}	3.2×10^{-6}	5.1×10^{-6}	1.1×10^{-6}
$3{:}10^3$ (0–3 nm region)	8.0×10^{-6}	6.1×10^{-6}	5.0×10^{-6}	1.9×10^{-6}
$1{:}10^3$ (3–6 nm region)	7.1×10^{-6}	2.1×10^{-6}	6.3×10^{-6}	1.3×10^{-6}
$2{:}10^3$ (0–3 nm region)	7.8×10^{-6}	3.7×10^{-6}	6.1×10^{-6}	1.2×10^{-6}
$3{:}10^3$ (3–6 nm region)	8.3×10^{-6}	6.3×10^{-6}	5.9×10^{-6}	1.9×10^{-6}
$1{:}10^3$ (6–9 nm region)	5.6×10^{-6}	1.5×10^{-6}	4.3×10^{-6}	1.1×10^{-6}
$2{:}10^3$ (0–3 nm region)	7.8×10^{-6}	2.8×10^{-6}	4.2×10^{-6}	1.2×10^{-6}
$3{:}10^3$ (6–9 nm region)	9.9×10^{-6}	2.9×10^{-6}	4.1×10^{-6}	1.3×10^{-6}

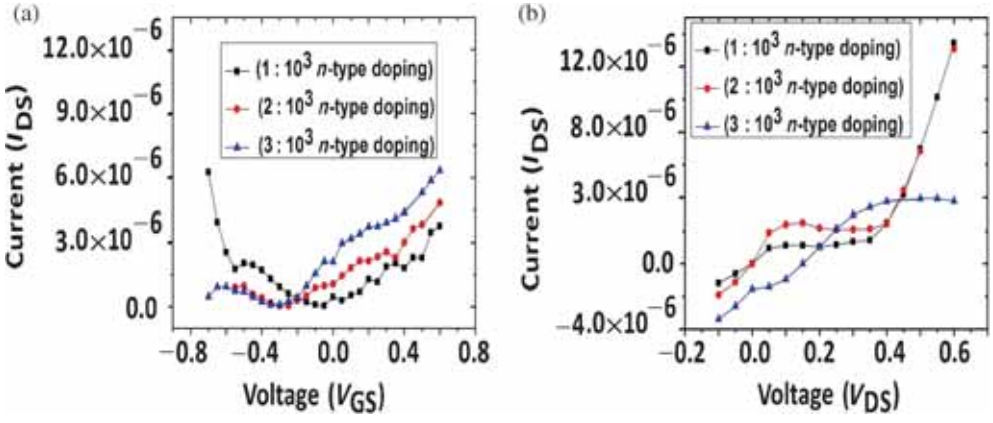

Figure 5. Current I_{DS} in amperes and voltages V_{GS} and V_{DS} in volts. (**a**) Transfer and (**b**) output characteristics of GNR-SBFET with n-type doping in 3–6 nm (center region) region of a 9 nm channel.

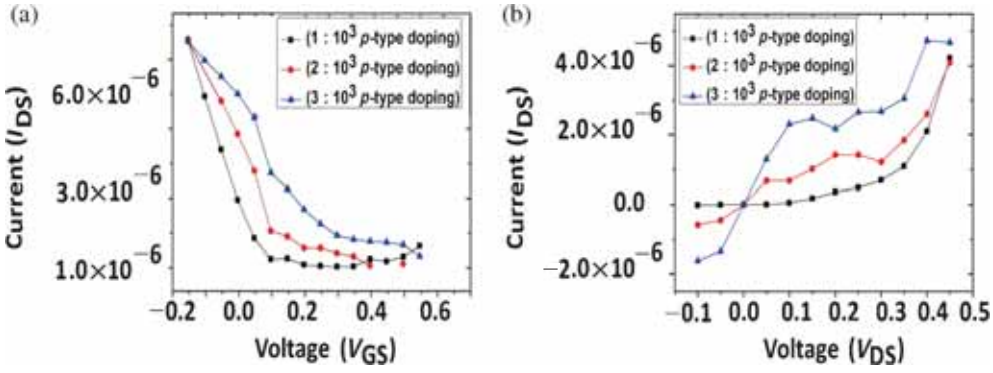

Figure 6. Current I_{DS} in amperes and voltages V_{GS} and V_{DS} in volts. (**a**) Transfer and (**b**) output characteristics of GNR-SBFET with p-type doping in 3–6 nm (center region) region of a 9 nm channel.

I_{on} current increases compared to undoped and low-doped devices, however, I_{off} current remain almost same due to which a marginal increment in I_{on}/I_{off} ratio is observed. Smaller I_{on} current suggests a barrier near contact interface which can be lowered by doping this region. From table 2, we observed that when impurity concentration in region 6–9 nm (drain side) is low, then I_{on} current is low, which means that there is barrier at the drain interface, on increasing impurity concentration at the drain interface, barrier reduces and I_{on} current increases due to which I_{on}/I_{off} ratio increases.

Similarly, extending the above analysis to 3–6 nm region (middle region), it was observed that doping this region has very small effect on I_{on} current when compared to doping 6–9 nm region (drain side). From table 2, it is also observed that n-type doping shows better switching than p-type doping and also gives a better swing in comparison with p-type doped channel device. At $V_{DS} = 0.5$ V, there is no large variation in on- and off-currents (see table 2), which means that for high doping concentrations better transistor characteristics can be obtained at lower supply voltages (e.g., at $V_{DS} = 0.2$ V).

Further, we also introduced n-type increasing step doping profile in the channel ($1{:}10^3$ in 0–3 nm range, $2{:}10^3$ in 3–6 nm range and $3{:}10^3$ in 6–9 nm range) and obtained its transfer and output characteristics which are shown in figures 9 and 10. Similarly, we also introduced n-type decreasing step doping in 0–9 nm channel region ($3{:}10^3$ in 0–3 nm range, $2{:}10^3$ in 3–6 nm range and $1{:}10^3$ in 6–9 nm range) to observe its effect on transistor characteristics (see figures 9 and 10). In case of increase step doping case, drain is a good collector (low barrier from high doping), but limited electrons are collected due to source being a bad emitter (high barrier due to low doping). In case of step increase doping in figure 9a, on-current rises with a good slope and gives good on-current (at $V_{DS} = 0.2$ V) with good saturation and stable output for saturation condition (see figure 10a), while in step decrease doping case, the on-current increases very slowly and equivalent high current is achieved at higher bias voltages (see figures 9b and 10b) in comparison with step increase doping case. More drive current is possible in increased doping structure. The output characteristics of increase step doping are better in comparison with decrease

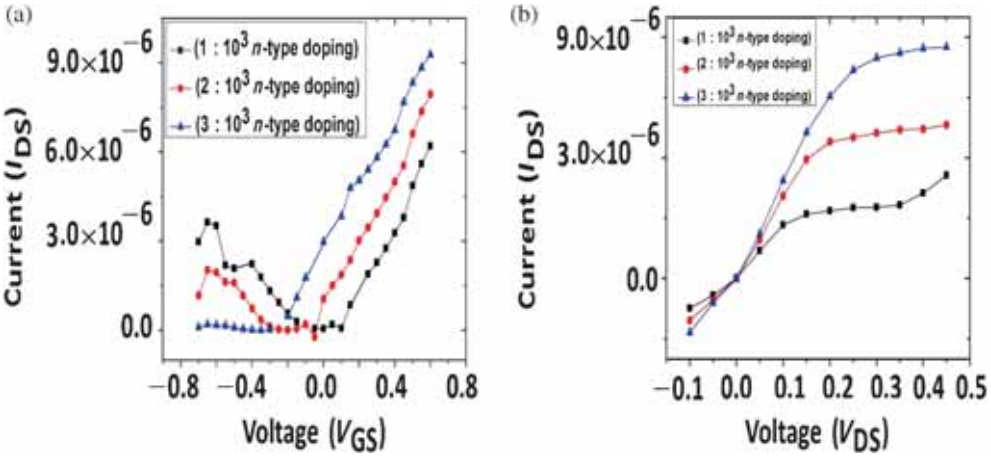

Figure 7. Current I_{DS} in amperes and voltages V_{GS} and V_{DS} in volts. (**a**) Transfer and (**b**) output characteristics of GNR-SBFET with n-type doping in 6–9 nm (near drain) region of a 9 nm channel.

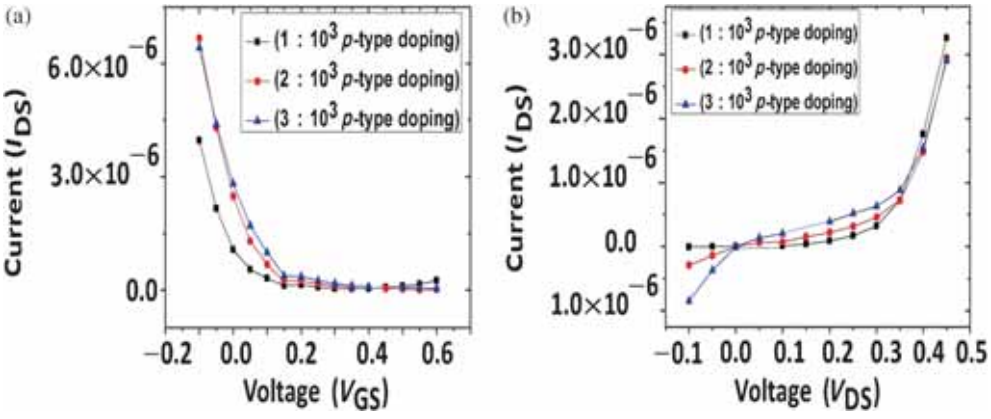

Figure 8. Current I_{DS} in amperes and voltages V_{GS} and V_{DS} in volts. (**a**) Transfer and (**b**) output characteristics of GNR-SBFET with p-type doping in 6–9 nm (near drain) region of a 9 nm channel.

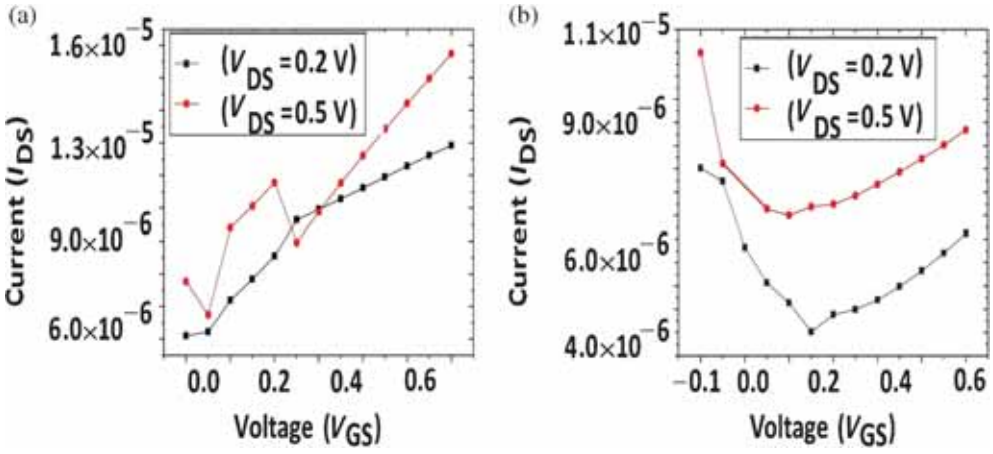

Figure 9. Current I_{DS} in amperes and voltage V_{GS} in volts. (**a**) Transfer characteristics of GNR-SBFET with n-type increased step doping in 0–3, 3–6 and 6–9 nm regions of a 9 nm channel. (**b**) Transfer characteristics of GNR-SBFET with n-type decreased step doping in 0–3, 3–6 and 6–9 nm regions of a 9 nm channel.

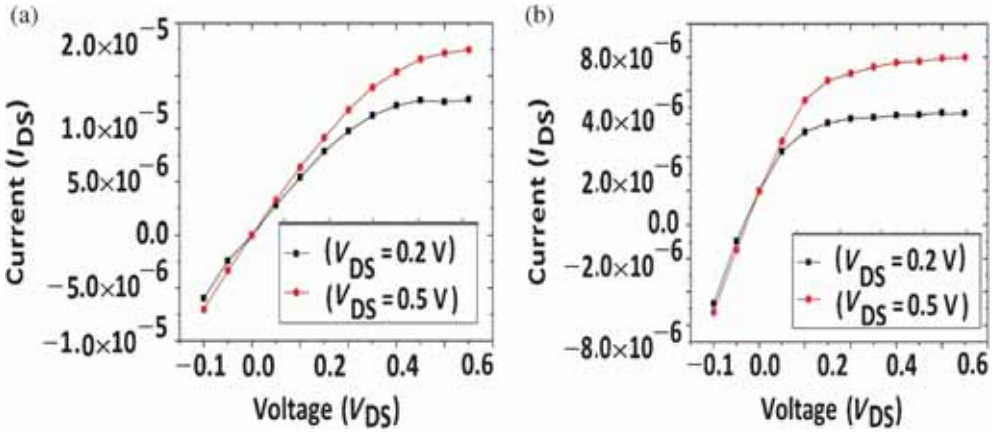

Figure 10. Current I_{DS} in amperes and voltage V_{DS} in volts. (**a**) Output characteristics of GNR-SBFET with n-type increased step doping in 0–3, 3–6 and 6–9 nm regions of a 9 nm channel. (**b**) Output characteristics of GNR-SBFET with n-type step decreased doping in 0–3, 3–6 and 6–9 nm regions of a 9 nm channel.

Table 3. I_{on} and I_{off} currents of doped GNR channel with step doping at $V_{DS} = 0.2$ V and $V_{DS} = 0.5$ V.

Doping concentration	I_{on} (Amp) $V_{DS} = 0.2$ V	I_{on} (Amp) $V_{DS} = 0.5$ V	I_{off} (Amp) $V_{DS} = 0.2$ V	I_{off} (Amp) $V_{DS} = 0.5$ V
1:10^3, 1:10^3, 1:10^3 (0–3, 3–6, 6–9 nm regions)	5.8×10^{-6}	9.1×10^{-6}	3.8×10^{-6}	7.1×10^{-6}
3:10^3, 3:10^3, 3:10^3 (0–3, 3–6, 6–9 nm regions)	1.3×10^{-5}	2.8×10^{-5}	9.8×10^{-6}	1.1×10^{-5}
1:10^3, 2:10^3, 3:10^3 (0–3, 3–6, 6–9 nm regions)	8.7×10^{-6}	1.1×10^{-5}	6.1×10^{-6}	7.3×10^{-6}
3:10^3, 2:10^3, 1:10^3 (0–3, 3–6, 6–9 nm regions)	4.8×10^{-6}	8.1×10^{-6}	4.1×10^{-6}	7.1×10^{-6}

step doping case (see figure 10). We observed that n-type step-doped channel (increasing doping profile from source to drain) gives further better on-current and output characteristics (see table 3) in comparison with undoped and uniformly-doped channel device (see table 3) and also gives better saturation condition at its output.

4. Conclusion

We performed a simulation study on GNR-SBFET and investigated its transfer and output characteristics by varying the channel doping in the NEGF quantum simulator. Comparison of the I_{on}/I_{off} ratio in different parts of the channel

shows that I_{on}/I_{off} ratio is larger when drain side region is *n*-type, doped. *n*-type-doped device gives better characteristics compared to *p*-type-doped device. Saturation condition is an important transistor characteristic which was observed in *n*-type-doped device structure. For high doping concentrations, better transistor characteristics can be obtained at lower supply voltages. Characteristics can be improved further by introducing step doping profile in the channel. From these investigations we can say that if GNR-SBFET is to be used in variable switching and amplification applications, increasing step doping (from source to drain) in the channel of GNR-SBFET with *n*-type impurity having higher concentration near drain side can give better on-current and saturation condition.

References

[1] Novoselov K S, Geim A K, Morozov S V, Jiang D, Zhang Y, Dubonos S V *et al* 2004 *Science* **306** 666

[2] Berger C, Song Z M, Li T B, Li X B, Ogbazghi A Y, Feng R *et al* 2004 *J. Phys. Chem. B* **108** 19912

[3] Han M Y, Ozyilmaz B, Zhang Y B and Kim P 2007 *Phys. Rev. Lett.* **98** 206805

[4] Nakada K, Fujita M, Dresselhaus G and Dresselhaus M S 1996 *Phys. Rev. B* **54** 17954

[5] Barone V, Hod O and Scuseria G E 2006 *Nano Lett.* **6** 2748

[6] Son Y W, Cohen M L and Louie S G 2008 *Phys. Rev. Lett.* **97** 216803

[7] White C T, Li J W, Gunlycke D and Mintmire J W 2007 *Nano Lett.* **7** 825

[8] Fiori G and Iannaccone G 2007 *IEEE Electr. Device L.* **28** 760

[9] Guan X, Zhang M, Liu Q and Yu Z 2010 *IEDM Tech. Dig.* 761

[10] Datta S 2000 *Superlattices Microstruct.* **28** 253

[11] http://vides.nanotcad.com

[12] Lemme M C, Echtermeyer T J, Baus M and Kurz H 2012 *IEEE Electr. Device L.* **28** 282

[13] Li X L, Wang X R, Zhang L, Lee S W and Day H J 2008 *Science* **319** 1229